The low-temperature self-consistent g factor for heterostructures in strong magnetic fields

1995 J. Phys.: Condens. Matter 7 4419

(http://iopscience.iop.org/0953-8984/7/23/011)

J. Phys.: Condens. Matter 7 (1995) 4419–4432. Printed in the UK

The low-temperature self-consistent g factor for heterostructures in strong magnetic fields

W Xu†, P Vasilopoulos‡, M P Das† and F M Peeters§

† Department of Theoretical Physics, RSPhysSE, The Australian National University, Canberra, ACT 0200, Australia

‡ Department of Physics, Concordia University, Montreal, Quebec, Canada H3G 1M8

§ Departement Natuurkunde, Universiteit Antwerpen (UIA), Universiteitsplein 1, B-2610 Antwerpen, Belgium

Received 31 January 1995

Abstract. A low-temperature self-consistent calculation of the density of states (DOS) and of the exchange-enhanced g factor is presented for heterostructures in a strong transverse magnetic field. Landau level (LL) mixing in the self-energy, the energy shift, and the interaction of an electron with remote and background impurities, with piezoelectric and acoustic phonons, and with other electrons is taken into account. The main results are (i) a spin-split LL structure, (ii) the effective g factor (g^*) is enhanced in samples with high mobility, (iii) the LL width and the g^* factor oscillate with magnetic field, and (iv) a significant background DOS can be observed at weak magnetic fields, high electron energy, and low temperatures, for certain remote to background impurity concentration ratios. In addition, g^* is evaluated as a function of mobility, spacer thickness, and temperature. The specific heat is also evaluated. The results for the LL width, the enhanced g^* factor, and the specific heat are in line with those suggested and reported by recent experiments.

1. Introduction

Theoretical calculations [1, 2] and experimental measurements [3–5] show that the spin g factor (or effective spin-splitting Landé factor g^*) of a two-dimensional electron gas (2DEG) in a strong magnetic field B is enhanced by the exchange interaction. At low temperatures (T), g^* values up to 10 have been reported [5], i.e., much larger than the bulk value $g^* = 0.44$ for GaAs. The enhanced g^* factor results in spin-split Landau levels, saw-tooth Shubnikov–de Haas oscillations, and has a strong influence on the quantum Hall effect in the region between the plateaus [6]. Experimentally, the value of g^* can be determined using the coincidence technique [3] or by activation measurements [4].

Previous theoretical work on the exchange-enhanced g^* factor made the usual assumptions of a semielliptic [1], Lorentzian or Gaussian [3] shape of the DOS for electrons. Such an approach has given reasonable results for the dependence of g^* on B and on the electron density n_e. However, it has the following drawbacks: (i) the LL splitting resulting from an enhanced g^* is not included in the calculation and the energy shift is neglected, (ii) the dependence of g^* on the sample parameters is not explicit [2], and (iii) all these calculations were carried out in the $T \to 0$ limit. However, the exchange-enhanced g^* factor in a real device not only depends on the parameters, such as temperature and applied magnetic field, but also depends strongly on the shape of the DOS which is mainly determined by the electronic subband structure of the 2DEG and by the sample parameters

0953-8984/95/234419+14$19.50

such as electron density, ionized impurity distribution, and phonon modes. Some of these drawbacks have been avoided in a recent self-consistent calculation [7] in which, however, g^* was not determined self-consistently but taken as a parameter. As a result, no comparison with the experimentally determined g^* values could be attempted and its dependence on B, T, and the sample parameters could not be assessed. Therefore, the need is evident for a fully self-consistent evaluation of g^*.

In the present paper, we go beyond previous works by evaluating the Green function for the LLs, the self-energy for the electrons, and the g^* factor self-consistently. We perform a *low-temperature* calculation and take into account the energy shift, LL mixing in the self-energy, and the electron interaction with impurities and acoustic and piezoelectric phonons. The model is developed for a general 2DEG in section 2 and is followed by its application to an AlGaAs/GaAs heterojunction in section 3. The numerical results for spin-split LLs and exchange-enhanced g^* are presented and discussed in section 4 and remarks and conclusions are summarized in section 5.

2. Outline of the model

The Hamiltonian describing a 2DEG in a strong transverse magnetic field B is given by

$$H = H_0 + H_{e-e} + H_i + H_{e-i} + H_p + H_{e-p} \tag{1}$$

where H_i (H_p) is the impurity (phonon) Hamiltonian and H_{e-i}, H_{e-p}, and H_{e-e} are the electron impurity, electron–phonon, and electron–electron interaction Hamiltonians, respectively. Further,

$$H_0 = [p_x^2 + (p_y + eBx)^2 + p_z^2]/2m^* + U(z) \tag{2}$$

is the free-electron Hamiltonian in a magnetic field in the Landau gauge, m^* the effective mass, and $U(z)$ the confining potential along the z direction. The normalized eigenfunctions of equation (2) are given by

$$|k_y, N, n\rangle = (2^N N! \pi^{1/2} l L_y)^{-1/2}\, e^{ik_y y - \xi^2/2} H_N(\xi) \psi_n(z)$$

with $H_N(x)$ the Hermite polynomials, N (n) the index of the Nth LL (nth electronic subband), $l = (\hbar/eB)^{1/2}$ the magnetic length or equivalently the radius of the ground state ($N = 0$) cyclotron orbit, and $\xi = (x + l^2 k_y)/l$. The corresponding energy eigenvalues are $E_{Nn} = E_N + \varepsilon_n$ where $E_N = (N + \frac{1}{2})\hbar\omega_c$ is the energy of the Nth LL with $N = 0, 1, 2, \ldots$, $\omega_c = |e|B/m^*$ the cyclotron frequency, and ε_n the energy of the nth electronic subband. In the present paper, we include the effect of spin in the electron–electron interaction Hamiltonian, which is equivalent to including the spin term in the free-electron Hamiltonian because the spin operator σ commutes with the Hamiltonian.

The Green function, corresponding to (1) and (2), for the Nth Landau level in the nth electric subband is given by

$$G_{Nn\sigma}(E) = \frac{1}{\bar{E}_{Nn\sigma} - \Sigma_{Nn}(E)} \tag{3}$$

where $\bar{E}_{Nn\sigma} = E - E_{Nn} - \sigma E_{Nn}^s - \mu^*$, E is the electron energy, μ^* the chemical potential (or Fermi energy), and $\sigma = \pm 1$ the spin index. The spin energy E_{Nn}^s is

$$E_{Nn}^s = g_{Nn}^* \mu_B B = g_0 \mu_B B + \Sigma_{Nn\downarrow} - \Sigma_{Nn\uparrow} \tag{4}$$

where g_{Nn}^* is the effective spin-splitting (Landé) factor for the Nth LL in the nth subband, μ_B the Bohr magneton, g_0 the bare g factor, and $\Sigma_{Nn\sigma}$ the spin contribution to the electron

self-energy. The self-energy for electrons in the Nth LL and the nth subband, $\Sigma_{Nn}(E)$, is

$$\Sigma_{Nn}(E) = \Sigma_{Nn}^{e-i}(E) + \Sigma_{Nn}^{e-p}(E) = \Delta_{Nn}(E) - (i/2)\Gamma_{Nn}(E). \tag{5}$$

The real part $\Delta_{Nn}(E)$ results in an energy shift and the imaginary part $\Gamma_{Nn}(E)/2$ determines the width of the Landau level.

Substituting equation (5) into equation (3), the real and imaginary parts of the Green function for the Landau levels are obtained, respectively, as

$$\mathrm{Re}\, G_{Nn\sigma}(E) = \frac{\bar{E}_{Nn\sigma} - \Delta_{Nn}(E)}{[\bar{E}_{Nn\sigma} - \Delta_{Nn}(E)]^2 + [\Gamma_{Nn}(E)/2]^2} \tag{6a}$$

and

$$\mathrm{Im}\, G_{Nn\sigma}(E) = -\frac{\Gamma_{Nn}(E)/2}{[\bar{E}_{Nn\sigma} - \Delta_{Nn}(E)]^2 + [\Gamma_{Nn}(E)/2]^2}. \tag{6b}$$

The DOS for electrons in the Nth Landau level and the nth electric subband is then

$$D_{Nn}(E) = -\frac{1}{2\pi^2 l^2} \sum_{\sigma=\pm 1} \mathrm{Im}\, G_{Nn\sigma}(E). \tag{7}$$

To evaluate the Green function we need to know the electron self-energy. For a 2DEG, the latter is mainly determined by the electron's interaction with ionized impurities, phonons, and with other electrons; the last interaction contains exchange and correlation effects. In the self-consistent Born approximation (SCBA) [1, 7, 8] for the electron impurity (e–i) scattering, we have

$$\Sigma_{Nn}^{e-i}(E) = \sum_{N',n',q,\sigma=\pm 1} |u_{n'n}^{e-i}(q)|^2 C_{N'N}(u) G_{N'n'\sigma}(E) \tag{8a}$$

where $|u_{n'n}^{e-i}(q)|^2$ is the square of the electron impurity interaction matrix element, $q = (q_x, q_y)$, $u = l^2q^2/2$, and $C_{N,N+J}(u) = [N!/(N+J)!]u^J e^{-u}[L_N^J(u)]^2$, with $L_N^J(u)$ the associated Laguerre polynomials. Since in most experiments the enhancement of g^* is measured at low temperatures, we may neglect the electron interaction with optical phonons and consider only the interaction with acoustic and piezoelectric phonons. Considering only one-phonon absorption and emission processes and applying the quasielastic scattering approximation in the long-wavelength range, the self-energy induced by electron–acoustic phonon (e–a) scattering is obtained as [7]

$$\Sigma_{Nn}^{e-a}(E) = \sum_{N',n',Q,\sigma=\pm 1} \left(\frac{2k_B T}{\hbar\omega_Q}\right) |u_{n'n}^{e-a}(Q)|^2 C_{N',N}(u) G_{N'n'\sigma}(E) \tag{8b}$$

where $|u_{n'n}^{e-a}(Q)|^2$ is the square of the electron–phonon interaction matrix element, $Q = (q, q_z)$, and $\hbar\omega_Q$ is the phonon energy.

For AlGaAs/GaAs heterojunctions, the high electron density in the conduction channel ($n_e \sim 10^{11}$ cm^{-2} normally) implies that the effect of correlations can be neglected. Considering only the exchange effect, the screened Hartree–Fock approximation [1] can be applied to evaluate the spin self-energy using

$$\Sigma_{Nn\sigma} = \sum_{N',n',q} |u_{n'n}^{e-e}(q)| C_{N',N}(u) \nu_{N'n'\sigma} \tag{8c}$$

with $|u_{n'n}^{e-e}(q)|$ the electron–electron interaction matrix element, and

$$\nu_{Nn\sigma} = -\frac{1}{\pi} \int_{-\infty}^{\infty} \mathrm{d}E\ f(E)\, \mathrm{Im}\, G_{Nn\sigma}(E) \tag{9}$$

the filling factor of the spin-split Landau level; $f(E) = [e^{(E-\mu^*)/k_BT} + 1]^{-1}$ is the Fermi–Dirac function. The chemical potential μ^* is determined by the electron number conservation

$$n_e = \frac{1}{2\pi l^2} \sum_{N,n,\sigma=\pm 1} \nu_{Nn\sigma} \tag{10}$$

where n_e is the electron density of the 2DEG.

Introducing the squares of the interaction matrix element for electron interaction with ionized impurities (im), deformation potential (ac) acoustic phonons, and piezoelectric phonons in longitudinal (pl) and transverse (pt) branches, the self-energy is given as [7]

$$\Sigma_{Nn}(E) = \sum_{N',n',\sigma=\pm 1} (W^{\text{im}}_{N'Nn'n} + W^{\text{ac}}_{N'Nn'n} + W^{\text{pl}}_{N'Nn'n} + W^{\text{pt}}_{N'Nn'n}) G_{N'n'\sigma}(E). \tag{11}$$

The forms of $W^{\text{i}}_{N'Nn'n}$ for scattering by different mechanisms are given by (8) of [7]. Further, using the electron–electron interaction matrix element [1], the spin self-energy, which enters the Green function in equation (11), is obtained as

$$\Sigma_{Nn\sigma} = \frac{e^2}{\kappa} \sum_{N',n'} \nu_{N'n'\sigma} \int_0^\infty \mathrm{d}q \; C_{N'N}(u) \sum_\gamma H_{\beta\gamma}(q) \epsilon^{-1}_{\beta\gamma}(q) \tag{12}$$

where $\beta, \gamma = (n'n)$, κ is the dielectric constant, $\epsilon^{-1}_{\beta\gamma}(q)$ is the $\beta\gamma$ matrix element of the inverse dielectric function when only screening in the subbands ε_n is included. The form factor is given by

$$H_{\beta\gamma}(q) = H_{m'mn'n}(q) = \int \mathrm{d}z_1 \int \mathrm{d}z_2 \; \psi^*_{m'}(z_1)\psi_m(z_1)\psi^*_{n'}(z_2)\psi_n(z_2)\, e^{-q|z_1 - z_2|}. \tag{13}$$

To proceed, we need the electron wavefunction, occupancy of the nth subband, and the impurity concentrations. We specify them in the following section.

3. Application to AlGaAs/GaAs heterojunctions

In typical AlGaAs/GaAs heterojunctions only the lowest electronic subband is occupied for electron densities less than 6×10^{11} cm^{-2}. In this case one can use the triangular potential well approximation and describe the confinement with the standard variational wave function [1]. Further, the impurity scattering is mainly due to remote ionized impurities within a narrow space charge layer (because of depletion effects [10]) with a concentration N_I^r at a distance d_s (spacer thickness) from the interface between AlGaAs and GaAs and from background impurities with a concentration N_I^b in the GaAs region. These impurity concentrations and distributions are not well known; we model them using $n_i^r(z_a)$ and $n_i^b(z_a)$ given by

$$n_i^r(z_a) = N_I^r \, \delta(z_a + d_s) \qquad n_i^b(z_a) = N_I^b \Theta(z_a). \tag{14}$$

With regard to screening within the subband ε_0, we employ the random phase approximation appropriate for high electron densities and low temperatures. Screening within the LLs has been taken into account in [8] but here we neglect it.

With all these remarks and measuring the energy from $E - \varepsilon_n - \mu^*$, the subband index n can be dropped, $E - \varepsilon_0 - \mu^*$ is replaced by E, and the equations in previous section simplify considerably. For completeness, we give the probabilities $W^{\text{i}}_{N'N}$, obtained in [7], in a simplified notation. With $X = (1+x)^3$, $Y = 3x^2 + 9x + 8$, and $s = l^2 b^2 x^2/2$, they read

(i) for scattering by remote impurities

$$W^{\mathrm{ir}}_{N'N} = \frac{2\pi e^4 N_{\mathrm{I}}^{\mathrm{r}}}{\kappa^2}\int_0^\infty \mathrm{d}x\ \frac{x\,\mathrm{e}^{-2bd_{\mathrm{s}}x}}{[xX + a_{\mathrm{e}}(x)Y]^2} C_{N'N}(s) \tag{15a}$$

where $b = [(48\pi m^* e^2/\kappa\hbar^2)(N_{\mathrm{depl}} + \frac{11}{32}n_{\mathrm{e}})]^{1/3}$, N_{depl} is the depletion charge density, and

$$a_{\mathrm{e}}(x) = (m^* e^2/4\kappa\hbar^2 b)\int_0^1 \mathrm{d}y/[A\,\mathrm{e}^{\epsilon_x(1-y^2)} + 1]$$

with $A = [\exp(\pi\hbar n_{\mathrm{e}}/(m^* k_{\mathrm{B}}T)) - 1]^{-1}$ and $\epsilon_x = \hbar^2 b^2 x^2/(8m^* k_{\mathrm{B}}T)$;

(ii) for scattering by background impurities

$$W^{\mathrm{ib}}_{N'N} = \frac{\pi e^4 N_{\mathrm{I}}^{\mathrm{b}}}{2b\kappa^2}\int_0^\infty \mathrm{d}x\ \frac{Z_1}{[xX + a_{\mathrm{e}}(x)Y]^2} C_{N'N}(s) \tag{15b}$$

where $Z_1 = 3x^5 + 18x^4 + 48x^2 + 24x + 2$;

(iii) for scattering by acoustic phonons

$$W^{\mathrm{ac}}_{N'N} = \frac{3bE_{\mathrm{D}}^2 m^* \omega_{\mathrm{c}} k_{\mathrm{B}} T}{32\pi\hbar\rho v_{\mathrm{l}}^2} \tag{15c}$$

where E_{D} is the deformation potential constant, ρ is the density of the material, and v_{l} is the longitudinal sound velocity;

(iv) for scattering by longitudinal piezoelectric phonons

$$W^{\mathrm{pl}}_{N'N} = 9P_{\mathrm{l}}\int_0^\infty \mathrm{d}x\ \frac{2X + 6x^2 - 1}{X^{4/3}} C_{N'N}(s) \tag{15d}$$

where $P_{\mathrm{l}} = \pi b e^2 e_{14}^2 k_{\mathrm{B}}T/16\kappa^2\rho v_{\mathrm{l}}^2$ with e_{14} the piezoelectric constant and κ the static dielectric constant; and

(v) for scattering by transverse piezoelectric phonons

$$W^{\mathrm{pt}}_{N'N} = P_{\mathrm{t}}\int_0^\infty \mathrm{d}x\ \frac{Z_2}{X^2} C_{N'N}(s). \tag{15e}$$

v_{t} and v_{l} are the transverse and longitudinal sound velocities, respectively, and $Z_2 = 6x^5 + 36x^4 + 82x^3 + 72x^2 + 78x + 13$.

As for the spin self-energy, the final result is

$$\Sigma_{N\sigma} = \frac{e^2 b}{8\kappa}\sum_{N'} \nu_{N'\sigma}\int_0^\infty \mathrm{d}x \frac{xY}{xX + a_{\mathrm{e}}(x)Y} C_{N',N}(s).$$

The loop of equations (6)–(15) is solved self-consistently for the Green function, the DOS, and the g^* factor. LL mixing is taken into account by summing over all N' in equation (11).

4. Numerical results and discussion

The results of this section pertain to AlGaAs/GaAs heterojunctions and the material parameters are those of GaAs: $m^*/m_{\mathrm{e}} = 0.0665$, with m_{e} the rest mass of the electron, $\kappa = 12.9$, density $\rho = 5.37$ g cm^{-3}, $v_{\mathrm{l}} = 5.29 \times 10^5$ cm s^{-1}, $v_{\mathrm{t}} = 2.48 \times 10^5$ cm s^{-1}, $e_{14} = 1.41 \times 10^7$ V cm^{-1}, and $E_{\mathrm{D}} = 10$ eV.

We also need the background and remote impurity concentrations N_I^b and N_I^r. We take N_I^b as a parameter. As for N_I^r, it can be determined from the low-temperature limit of the experimentally determined mobility at zero magnetic field μ_0. For fixed d_s we have [7]

$$\frac{1}{\mu_0} = \frac{4e^3 m^{*2} N_I^r}{\kappa^2 \hbar^3 n_e} \int_0^1 \frac{dy\, x}{\sqrt{2-y^2}} \frac{x\, e^{-2bd_s x} + \gamma_1 Z_3}{[xX + a_1 Y]^2} \tag{16}$$

with $\gamma_1 = N_I^b/4bN_I^r$, $Z_3 = 3x^5 + 18x^4 + 43x^3 + 48x^2 + 24x + 2$, $x = (8\pi n_e/b^2)^{1/2}(1-y^2)$, and $a_1 = m^* e^2/4\kappa\hbar^2 b$. The following parameters pertain to sample G148 from [4]: $n_e = 1.86 \times 10^{11}$ cm^{-2}, mobility at $T \to 0$ and $B = 0$ $\mu_0 = 10^4$ cm^2 V^{-1} s^{-1}, and $d_s = 400$ Å. A typical depletion charge density is $N_{depl} = 5 \times 10^{10}$ cm^{-2}. Using $N_I^b = 5.7 \times 10^{13}$ cm^{-3}, a typical background impurity density, and equation (16), we obtain $N_I^r = 5.5 \times 10^{11}$ cm^{-2}. This somewhat high value of N_I^r is a result of its approximate modelling by equation (14).

With respect to the numerical procedure, we use a two-step iteration technique to solve equations (6)–(15) self-consistently. First, we input a guessed spin energy E_N^s and then calculate the real and imaginary part of the self-energy over the energy range outside which both $\Gamma_N(E)$ and $\Delta_N(E)$ vanish. The iterative procedure is interrupted when $\max[|\Gamma_N^{j+1} - \Gamma_N^j|, |\Delta_N^{j+1} - \Delta_N^j|]$, i.e., when the maximum difference of $\Gamma_N(E)$ and $\Delta_N(E)$ for fixed E between two iteration steps j and $j+1$, is smaller than 10^{-8} meV. Secondly, using the obtained $\Gamma_N(E)$ and $\Delta_N(E)$ we evaluate the new spin energies E_N^s for different LLs. This iteration is interrupted when the maximum difference of E_N^s between two successive iteration steps is smaller than 10^{-3} meV. In all calculations we include the lowest ten LLs, i.e., we take $N = 0, 1, 2, \ldots, 9$. Including more LLs in the calculation affects only the results for weak magnetic fields. Since we do not assume any particular form for the DOS, numerical integrations are necessary to evaluate the filling factor and the chemical potential. These integrations are very CPU time consuming.

In figure 1 the real ($\Delta_N(E)$) and imaginary ($\Gamma_N(E)$) parts of the self-energy, for electrons in the lowest three LLs, are plotted as a function of the electron energy for different magnetic fields or filling factors $\nu = n_e h/eB$. The spin-split LL width and shift are clearly seen in strong B fields, e.g., when ν=1 and 1.5 in figures 1(a) and (b). At relatively low fields, as in figures 1(c) and (d), the influence of the spin splitting on the self-energy cannot be observed even for integer ν. The DOS corresponding to figure 1 is shown in figure 2. The spin-split LLs can be seen for all B fields of figure 1. The effect is more pronounced for the high B fields of figures 2(a) and (b), where sawtooth-shaped LLs have been observed. For the intermediate B field of figure 2(c) the total DOS shows a semielliptic shape whereas for the low B field of figure 2(d) a significant background DOS between different LLs results from [7] remote impurity scattering for small background impurity densities and intermediate spacer thickness. As can be seen, varying B leads to a rapid change of the shape of the LLs. In general, one cannot use a simple analytic form to model the DOS although in some cases, as in figures 2(a) and (c), a semielliptic DOS is sufficient. To the best of our knowledge, this is the first theoretical evaluation of the spin-split LL structure.

From the calculated DOS, we obtain the *actual width* of the LL ($\Gamma_{N\sigma}$) defined as the width of the DOS at half maximum. The LL width calculated from the DOS of figure 2 is shown in figure 3 as a function of magnetic field (or filling factor) for different LLs. $\Gamma_{N\sigma}$ oscillates strongly with $1/B$ (or ν) and the peaks are located at ν =1, 2, 3, ... The results show that the spin-up and spin-down LLs have roughly the same widths. That the width of the LLs oscillates with B was first suggested in [11] and was supported by experimental data of the heat capacity measured in an AlGaAs/GaAs-based 2DEG. To our knowledge, an LL width oscillating with B, as shown in figure 3, has not been reported so far.

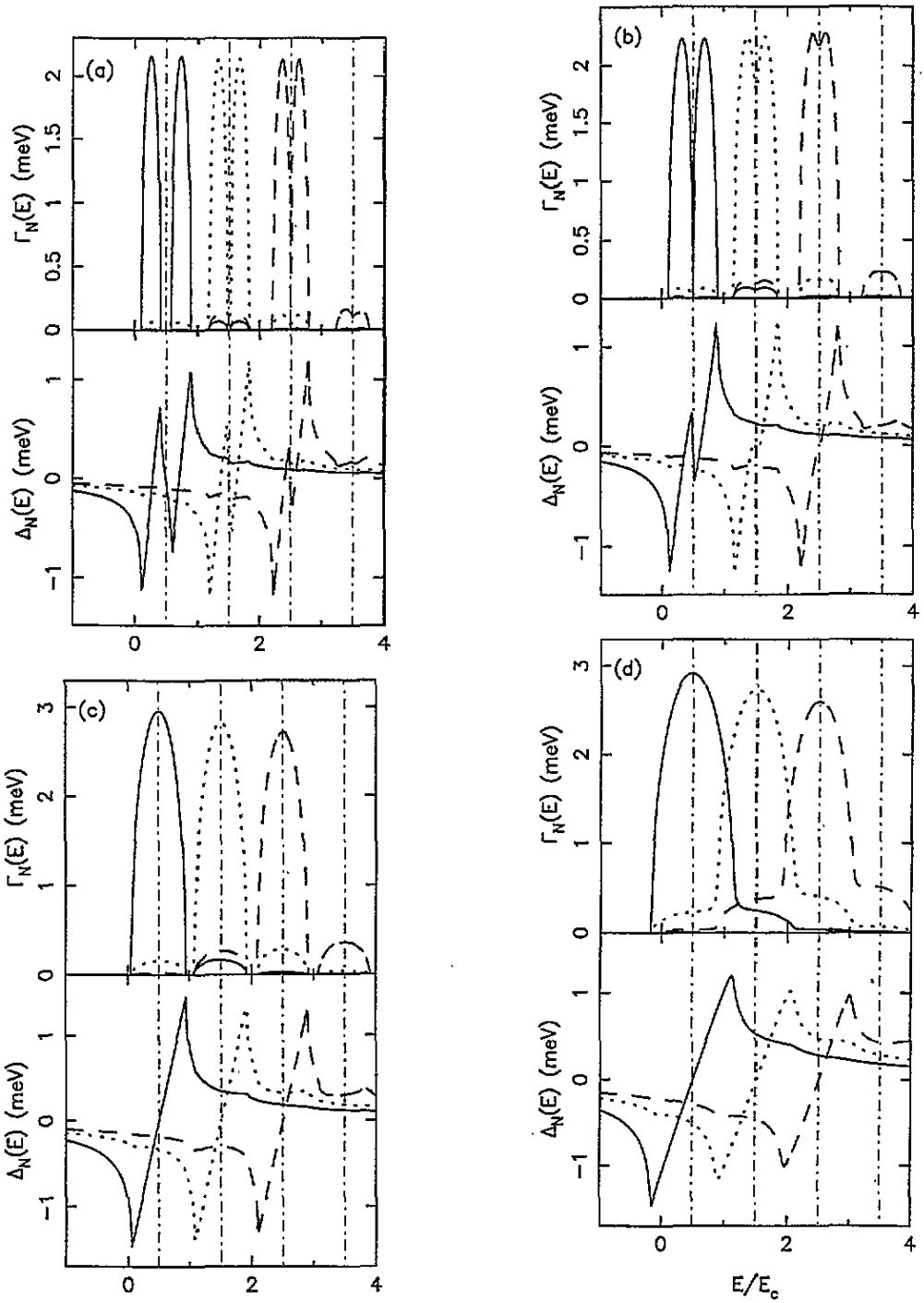

Figure 1. The real ($\Delta_N(E)$) and imaginary ($\Gamma_N(E)$) parts of the self-energy for electrons in the lowest three Landau levels (solid, dotted, and dashed curves: $N = 0$, 1, and 2 respectively) as a function of electron energy E in different magnetic fields; from (a) to (d): $B = 7.66$, 5.11, 3.83, and 2.55 T, corresponding to filling factors $\nu = n_e h/eB = 1$, 1.5, 2, and 3. The other parameters are: $T = 2.5$ K, $n_e = 1.86 \times 10^{11}$ cm^{-2}, $B = 0$ and $T \to 0$ mobility $\mu_0 = 10^4$ cm^2 V^{-1} s^{-1}, $N_I^b = 5.7 \times 10^{13}$ cm^{-3}, and $d_s = 400$ Å. The vertical thin dashed–dotted lines are the centres of the LLs $E_N = (N + \frac{1}{2})E_c$ with $E_c = \hbar\omega_c$.

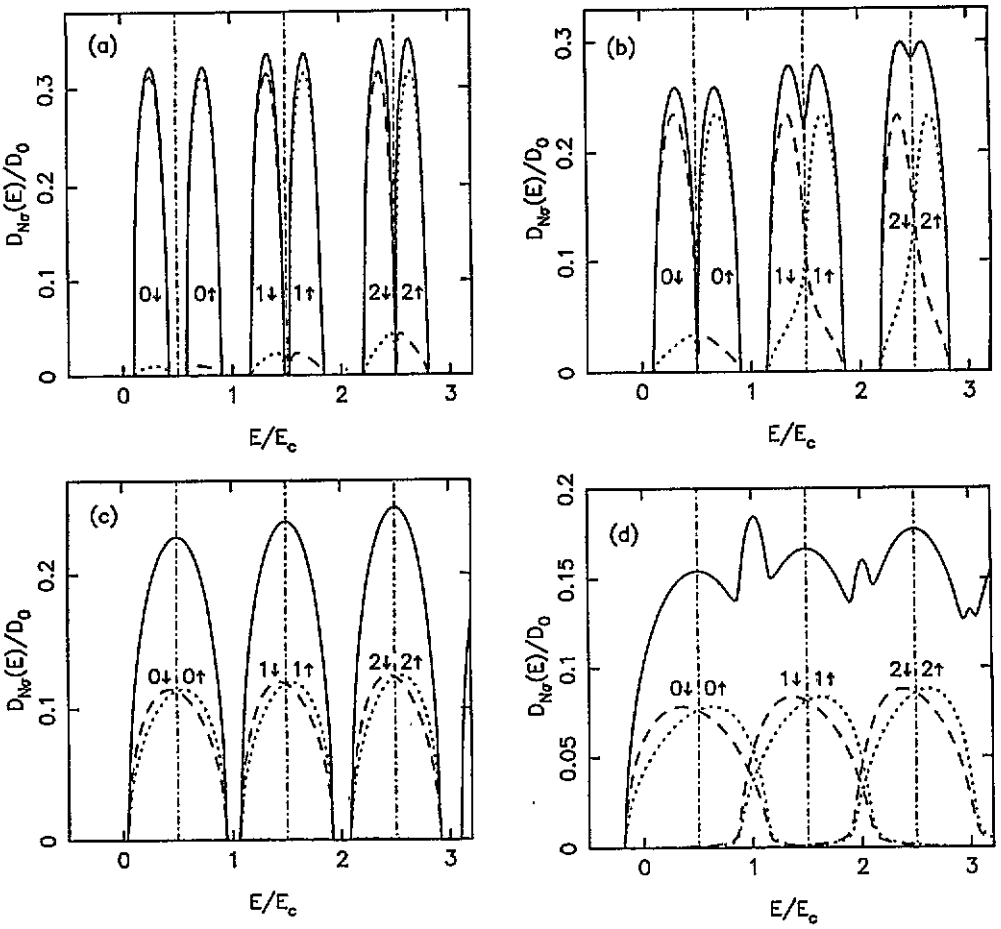

Figure 2. The density of states for spin-down (dashed curves) and spin-up (dotted curves) LLs along with the total DOS (solid curves $D(E) = \sum_{N,\sigma=\pm1} D_{N\sigma}(E)$) as a function of electron energy. The parameters are the same as in figure 1. The thin dashed–dotted curves are the same as in figure 1 and $D_0 = 2m^*/\hbar^2 = 1.75 \times 10^{11}$ cm^{-2} meV^{-1}.

The g factor for different LLs (g_N^*) and the chemical potential (μ^*, dotted curve), as a function of the magnetic field, are shown in figure 4. The oscillations of g_N^* with $1/B$ are clearly seen and the peaks (valleys) are *approximately* located at the odd (even) integer filling factors, i.e., at ν=1, 3, 5, ... (2, 4, 6, ...). The effect of the LL shift is to shift the peaks and valleys in the low-B regime as can be observed in figure 4. The physical reason for the oscillation of g_N^* with $1/B$ can be understood with the help of equation (4). When ν is an odd (even) integer, the Fermi level is located between the spin-up and spin-down LLs (between different-N LLs). From equation (4) we see that (i) when $\nu \to 1$, which implies that only the spin-down states of the $N = 0$ LL are occupied, i.e., $\Sigma_{0\uparrow} \ll \Sigma_{0\downarrow}$, this results in the strongest exchange interaction in the $N = 0$ LL and consequently in a maximum in the g factor; (ii) with decreasing B when ν varies from one to two, the spin-up states of the $N = 0$ LL are occupied and $\Sigma_{0\uparrow}$ increases with decreasing B; this weakens the exchange interaction and consequently the g factor decreases with B; (iii) when $\nu \to 2$ the spin-up and spin-down states of the $N = 0$ LL are occupied. The weakest exchange interaction occurs when the $N = 0$ LL is fully occupied ($\Sigma_{0\downarrow} - \Sigma_{0\uparrow} \approx 0$) and the minimum value of

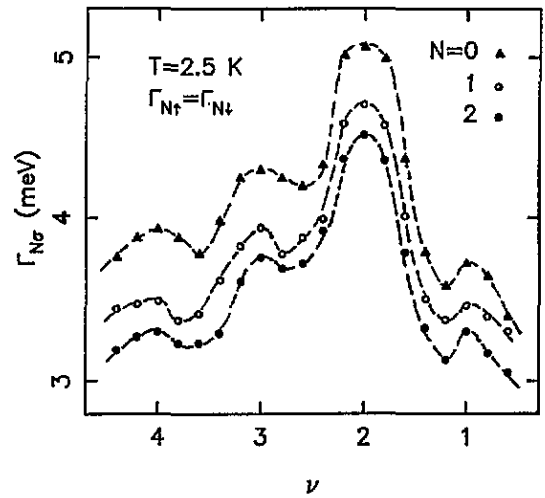

Figure 3. The Landau level width, at half-maximum DOS, as a function of the magnetic field ($\nu = n_e h/eB$). $\Gamma_{N\uparrow} \simeq \Gamma_{N\downarrow}$ for different LLs and the parameters are the same as those in figure 1.

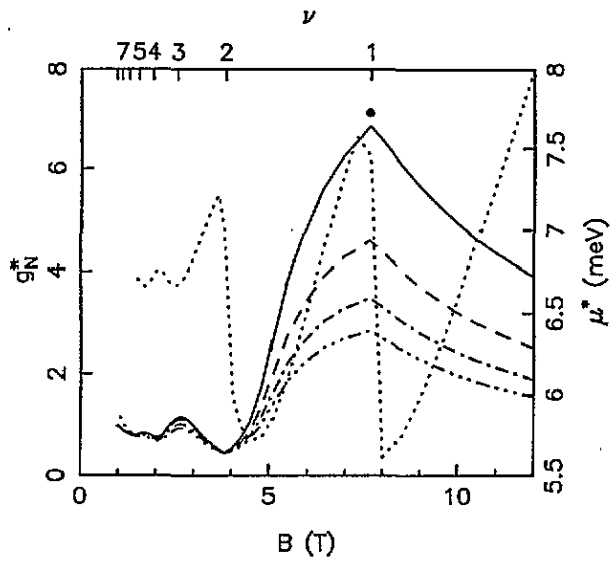

Figure 4. Magnetic field dependence of the g factor in different LLs (solid, dashed, dashed–dotted and dashed–dotted–dotted–dotted curves: $N = 0, 1, 2$, and 3 respectively) and of the chemical potential (μ^*, dotted curve). The parameters are the same as those in figure 1. The solid circle is the experimental datum of [4].

g^* is reached; (iv) with further decrease of B the process is repeated and g^* exhibits an oscillating behavior as function of the magnetic field; (v) the enhancement of g^* is weaker at $\nu = 3$ than at $\nu = 1$ for the following reason. At $\nu = 3$ the $N = 0$ LL is entirely occupied, and fewer electrons in the $N = 1$ level will contribute less to the enhancement of g. An alternative explanation for the oscillations in g^* with B was presented in [1]. It can be seen from figure 4 that the spin energies in different LLs are different. We note that since the LL mixing is included in the calculation, i.e., all the intra- and inter-LL scattering processes

are taken into account, the extended tails of the DOS over a wide energy regime (see figure 2) result in which the exchange-enhanced g factor for different LLs can be observed in all magnetic fields. The effective g^* can be obtained by averaging over the contribution from all LLs in the manner

$$g^* = \sum_N g_N^* n_N / n_e \qquad n_N = \frac{1}{2\pi l^2} \sum_{\sigma=\pm 1} \nu_{N\sigma}. \tag{17}$$

n_N is the electron density in the Nth Landau level. The following results for g^* are obtained using equation (17). The solid dot in figure 4 is the result for g^* of sample G148 of [4] (the parameters of the other samples were not specified). As can be seen, the theoretical value $g^* = 6.8$ agrees well with the experimental one $g^* = 7.3$.

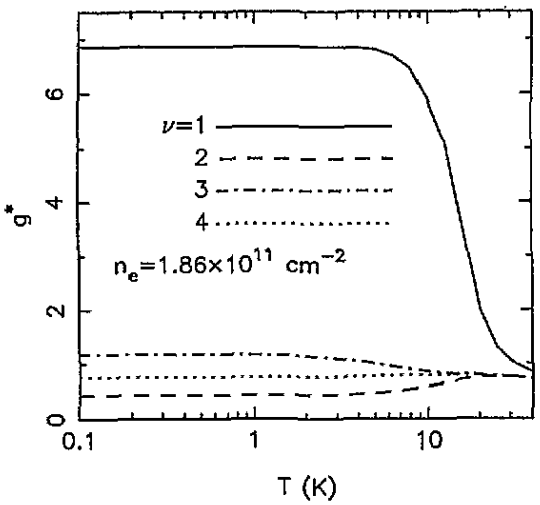

Figure 5. Temperature dependence of the effective g factor in different magnetic fields at fixed electron density. g^* is obtained using equation (17) and the other parameters are the same as those in figure 1.

The temperature dependence of g^* is presented in figure 5 for different B or ν at fixed n_e. It is apparent that the enhancement of g^* by the exchange interaction is essentially a low-temperature effect. At high temperatures, the enhancement of g^* is suppressed due to the thermal broadening of the Fermi function and the increase of phonon scattering that broadens the LLs further. In fact, the g factor is usually determined from activation measurements [4] at $T < 10$ K because the relation $\sigma_{xx} = \sigma_0 \exp(-\Delta E/k_B T)$ only holds for $\Delta E \gg k_B T$. Furthermore, our results show that, for $T < 5$ K, g^* is approximately constant and confirm the use of $E^s = g^* \mu_B B$ as an activation energy.

We now look at the influence of the sample parameters on the enhancement of g^*. Figure 6 shows g^* as a function of the $B = 0$ and $T \to 0$ mobility μ_0, determined by impurity scattering, for different B and fixed n_e. For low μ_0, the stronger impurity scattering will lead to a stronger broadening of the LLs and overlap of the tails of the DOS between the spin-up and spin-down levels; this weakens the exchange interaction and, consequently, lowers the value of g^*. Therefore, the enhancement of g^* can only be observed in high-mobility samples. The results shown in figure 6 demonstrate that the enhanced g^* can be observed at $\nu = 3$ for high-mobility samples when $\mu_0 > 200\,\mathrm{cm^2\,V^{-1}\,s^{-1}}$ which corresponds to the experimental situation in [4].

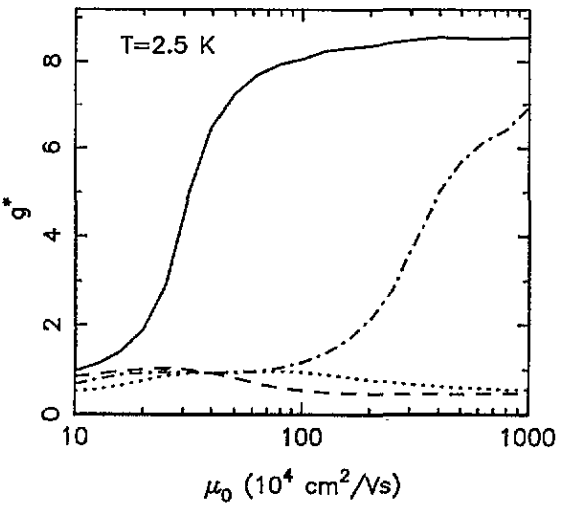

Figure 6. The effective g factor as a function of the zero-magnetic-field and low-temperature mobility for different magnetic fields at fixed electron density. The other parameters are the same as in figure 1 and the curves are labelled as in figure 5.

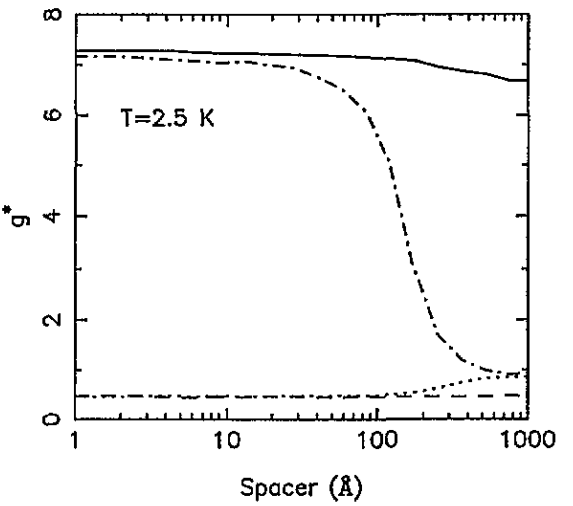

Figure 7. The effective g factor as a function of the spacer thickness for different magnetic fields at fixed electron density. The other parameters are the same as in figure 1 and the curves are labelled as in figure 5.

The dependence of g^* on the spacer thickness d_s is shown in figure 7 for fixed mobility μ_0. It is interesting to note that (i) for $\nu = 1$, g^* depends weakly on d_s when $d_s < 100$ Å whereas g^* decreases slowly with increasing d_s when $d_s > 100$ Å; (ii) a more pronounced enhancement of g^* at $\nu = 3$ can be obtained at shorter spacers $d_s < 40$ Å; and (iii) when $d_s > 40$ Å, g^* at $\nu = 3$ decreases rapidly with increasing d_s. The fact that a shorter d_s corresponds to a stronger remote impurity scattering implies that the latter has a weak influence on the enhancement of g^*, for $\nu = 1$, in contrast with its strong effect on g^* for $\nu = 3$. In [7] the background DOS between different LLs resulted from remote impurity scattering for small background impurity concentrations N_I^b and intermediate spacer

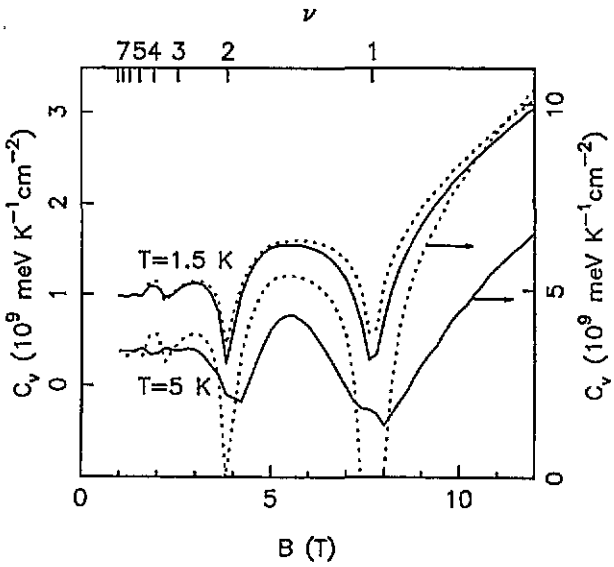

Figure 8. The specific heat as a function of the magnetic field for different temperatures. The solid curves are obtained using equation (18) and the dotted curves using $C_v = \pi^2 k_B^2 T D(\mu^*)/3$. The other parameters are the same as those in figure 1.

thicknesses ($d_s \sim 100$ Å). The presence of the background DOS at $d_s \sim 100$Å suppresses the enhancement of g^*.

Experimentally, g^* can be determined by activation measurements [4] or by using the coincidence technique [3]. At low temperatures the DOS can be deduced directly from measurements of the equilibrium thermodynamic qualities such as capacitance [12], magnetization [13], magnetic susceptibility [14], and specific heat [11, 15]. These experiments determine the DOS at the Fermi energy. Now we can calculate the specific heat C_v from the definition $C_v = \partial E_e/\partial T$ where

$$E_e = \int \mathrm{d}E\ E f(E) D(E)$$

is the free energy, $f(E)$ is the Fermi–Dirac function, and

$$D(E) = \sum_{N,\sigma=\pm 1} D_{N\sigma}(E)$$

is the total DOS. To enhance the accuracy of the numerical calculation, i.e., to avoid the derivative, we use equation (10) and assume that (i) n_e is independent of T, which is normally the case for AlGaAs/GaAs-based heterojunctions at $T < 100$ K, and (ii) the total DOS depends very weakly on T for low temperatures ($T < 10$ K). Thus, C_v can be calculated from

$$C_v = \frac{1}{T}\left(I_2 - \frac{I_1^2}{I_0}\right) \qquad I_n = -\int_{-\infty}^{\infty} \mathrm{d}E\ E^n D(E) \frac{\partial f(E)}{\partial E}. \tag{18}$$

The results for C_v, as a function of the magnetic field, are shown in figure 8 for different temperatures. We also show the results (dotted curves) obtained from the usual $T \to 0$ expression for the specific heat, $C_v = \pi^2 k_B^2 T D(\mu^*)/3$. It can be seen from figure 8 that (i) the calculated C_v has a shape similar to that observed experimentally; (ii) at very low temperatures, e.g., $T = 1.5$ K, the simple expression roughly reproduces the dependence

of C_v on B whereas at relatively high temperatures, e.g., $T = 5$ K, it is not adequate, see also [8]; and (iii) the background DOS in strong B (around $B = 7.5$ and 3.9 T) decreases with increasing temperature, since the dotted curves also represent the total DOS at the Fermi energy $D(\mu^*)$. A more significant background DOS between different LLs (including spin-split LLs) can be observed at lower temperatures.

5. Summary

We have evaluated self-consistently the exchange-enhanced g factor for strong magnetic fields and low temperatures. In the evaluation we have taken into account the Landau level mixing in the self-energy and the electron interaction with impurities, acoustic and piezoelectric phonons, and with other electrons. This is in sharp contrast with earlier treatments that took it as a parameter or were not as complete as the present one in that they did not take into account partially or totally the above-mentioned factors. To our knowledge, this is the most complete evaluation of the g factor and of the density of states. The main results are mentioned in the abstract.

In addition, we have presented results for the dependence of g^* on the magnetic field or filling factor, the temperature, and the sample parameters such as mobility and spacer thickness. To our knowledge, the results for the latter are entirely *new* [16]. The oscillations of g^* with magnetic field seen in experiments are present in our theory and simply explained by the spin-up and spin-down contributions to the self-energy. For lack of the pertinent sample parameters only a very limited comparison with experimental results could be made and the agreement is good. Further, with the self-consistent density of states we have evaluated the specific heat and found out, in agreement with experiments, that the usual low-temperature expression is inadequate for $T \geqslant 5$ K and strong magnetic fields.

Acknowledgments

The work of W X and M P D has been carried out on behalf of the Harry Triguboff AM Research Syndicate. The work of PV was supported by NSERC grant No OGPIN028 and that of FMP by the Belgian National Science Foundation.

References

[1] Ando T, Fowler A B and Stern F 1982 *Rev. Mod. Phys.* **54** 437
[2] Smith A P and MacDonald A H 1992 *Phys. Rev.* B **45** 8829
[3] Nicholas R J, Haug R J, von Klitzing K and Weimann G, 1988 *Phys. Rev.* B **37** 1294
[4] Usher A, Nicholas R J, Harris J J and Foxon C T 1990 *Phys. Rev.* B **41** 1129
[5] For a review see, e.g.,
Nicholas R J, Barnes D J, Clark R G, Haynes S R, Mallett J R, Suckling A M, Usher A, Harris J J, Foxon C T and Willett R 1989 *High Magnetic Fields in Semiconductor Physics II (Springer Series in Solid-State Sciences 86)* ed G Landwehr (Berlin: Springer) p 115
Goldberg B B, Heiman D and Pinczuk A 1990 *Surf. Sci.* **229** 137
[6] See, e.g.,
Allerman A A, Xu W, Hauser N and Jagadish C 1995 *J. Appl. Phys.* at press
[7] Xu W and Vasilopoulos P 1995 *Phys. Rev.* B **51** 1694
[8] Xie X C, Li Q P and Das Sarma S 1990 *Phys. Rev.* B **42** 7132
[9] See, e.g.,
Mahan G D 1981 *Many-Particle Physics* (New York: Plenum)
[10] Xu W and Mahanty J 1994 *J. Phys.: Condens. Matter* **6** 4745
[11] Wang J K, Campbell J H, Tsui D C and Cho A Y 1988 *Phys. Rev.* B **38** 6174

[12] Smith T P, Goldberg B B, Stiles P J and Heiblum M 1985 *Phys. Rev.* B **32** 2696
Song Aimin, Zheng Houzhi, Yang Fuhua and Li Yuexia 1993 *Proc. 21st Int. Conf. on the Physics of Semiconductors* (Singapore: World Scientific) p 247
[13] Eisenstein J P 1987 *Interfaces, Quantum Wells and Superlattices (NATO ASI 179)* (New York: Plenum) p 271
[14] Störmer H L, Haavasoja T, Narayamamurti V, Gossard A C, and Wiegmann W 1983 *J. Vac. Sci. Technol.* B **1** 423
[15] Gornik E, Lassning R, Strasser G, Störmer H L, Gossard A C and Wiegmann W 1985 *Phys. Rev. Lett.* 54 1820
[16] A brief account of some of the present results was presented at the *22nd Int. Conf. on the Physics of Semiconductors (Vancouver, 1994).*